




Surface modified PAMAM dendrimers with gallic acid inhibit, cell proliferation, cell migration and inflammatory response to augment apoptotic cell death in human colon carcinoma cells

Khushbu Priyadarshi , Kavita Shirsath , N. Bhargav Waghela , Anupama Sharma , Ajay Kumar & Chandramani Pathak

To cite this article: Khushbu Priyadarshi , Kavita Shirsath , N. Bhargav Waghela , Anupama Sharma , Ajay Kumar & Chandramani Pathak (2020): Surface modified PAMAM dendrimers with gallic acid inhibit, cell proliferation, cell migration and inflammatory response to augment apoptotic cell death in human colon carcinoma cells, Journal of Biomolecular Structure and Dynamics, DOI: [10.1080/07391102.2020.1802344](https://doi.org/10.1080/07391102.2020.1802344)

To link to this article: <https://doi.org/10.1080/07391102.2020.1802344>

 View supplementary material 

 Published online: 05 Aug 2020.


 Submit your article to this journal 

 View related articles 

 View Crossmark data 



Surface modified PAMAM dendrimers with gallic acid inhibit, cell proliferation, cell migration and inflammatory response to augment apoptotic cell death in human colon carcinoma cells

Khushbu Priyadarshi^{a#}, Kavita Shirsath^{a,b#}, N. Bhargav Waghela^a, Anupama Sharma^a, Ajay Kumar^c and Chandramani Pathak^a 

^aCell Biology Laboratory, School of Biological Sciences & Biotechnology, Indian Institute of Advanced Research, Gandhinagar, India;

^bDepartment of Zoology, The Maharaja Sayajirao University of Baroda, Vadodara, India; ^cDepartment of Zoology, Banaras Hindu University, Varanasi, India

Communicated by Ramaswamy H. Sarma

ABSTRACT

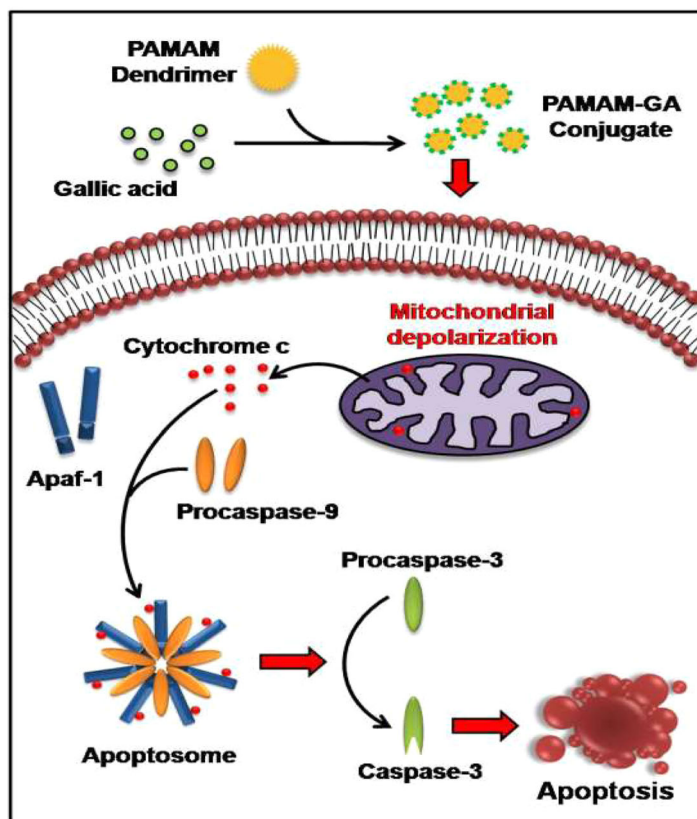
To overcome the obstacle of anti-cancer therapy significant attention has been drawn for improving drug delivery system. Since recent past, different approaches were applied using synthetic or natural derivatives for improving efficacy of anti-cancer drugs in cancer therapeutics. Gallic acid (GA) is a natural polyphenol, which exhibits a broad spectrum of biological activities, but its therapeutic application was limited due to poor bioavailability and toxicity. In the present study, we had conjugated the GA with PAMAM dendrimers and proposed the insights of molecular mechanism on inhibition of cell proliferation and programmed cell death through apoptotic pathway in human colon carcinoma cells. GA was chemically conjugated with 4.0 G PAMAM dendrimer at outer surface and characterized by different biophysical methods. We further examined its bioavailability, anti-cancer activity and explored the molecular mechanism of programmed cell death signaling in HCT116 cells. The results show that PAMAM-GA conjugate inhibits cell proliferation of different origin of cancer cells, improves cellular uptake of GA, inhibits colonogenic ability, restricts cancer cell migration by down regulating the expression of MMP-9, inhibits NF-kB activation and release of pro-inflammatory cytokines to manifest apoptotic cell death in HCT 116 cells rather than necrosis. On other hand, PAMAM-GA conjugate showed negligible cytotoxic response as compared to the free Gallic acid to the normal cells. In conclusion, findings of this study revealed that PAMAM-GA conjugate improves the bioavailability of GA and specificity towards cancer cells to manifest apoptotic cell death. This indispensable approach may be beneficial for the revolution of anti-cancer therapy.

ARTICLE HISTORY

Received 17 April 2020
Accepted 23 July 2020

KEYWORDS

Cancer; apoptosis; gallic acid; PAMAM dendrimers; PAMAM-GA conjugate



Gallic acid (GA) is conjugated with 4.0G PAMAM dendrimers via an amide linkage to form PAMAM-GA conjugate. The treatment of PAMAM-GA conjugate to cancer cells may induce loss of mitochondrial membrane potential with subsequent release of cytochrome c from mitochondrial intermembrane space into the cytosol where it forms apoptosome complex in association with Apaf-1 and Procaspase-9. This event leads to the proteolytic activation of caspase-3 and ultimately cells undergo toward apoptotic cell death.

Introduction

Colorectal cancer (CRC) is the third most commonly diagnosed cancer and fourth leading cause of cancer-related death worldwide. Biological and epidemiological studies of colorectal cancer indicate a clear association between chronic inflammation. Generally, chemotherapy is the first preferred anti-cancer therapy in many types of cancer, but within a short span of treatment exhibits adverse side effects along with systemic toxicities and immune surveillance that may cause failure of anti-cancer therapy. In the recent past, several strategies have been employed for the drug delivery system to improve cancer therapy. Since the recent past application of nanocarrier has drawn considerable attention to improve drug delivery system.

Dendrimers are emerging biopolymers, which have been considered as the versatile nanocarriers for drug delivery owing to their unique structure and presence of a multifunctional group on their surface (Sherje et al., 2018). Dendrimers have distinctive features, which may include the capability to improve the solubility, bioavailability, and permeability of drugs or desired molecules. They are unique biodegradable and non-immunogenic polymer. They have a

highly branched structure and suitable core moiety for entrapment or attachment of the drug. Among the other nanocarriers, dendrimers have distinctive features and emerging applications in nanomedicine (Kesharwani et al., 2014). Among all the dendrimers, PAMAM (Poly(amidoamine)) has drawn the attention for the application of the drug delivery system due to unique and versatile attractive features. Polyamidoamine (PAMAM) dendrimers possess free amine groups on their surface, which contribute to their enhanced cytoplasmic delivery via the proton-sponge mechanism. Besides these unique characteristics, their nanosize and highly aqueous nature confers excellent drug delivery properties (Esfand & Tomalia, 2001). PAMAM dendrimers are the first synthesized and commercialized dendrimers family. They are considered as ideal carriers for the delivery of therapeutic agents including anticancer drugs because of their small size, high aqueous solubility and a large number of chemically versatile surface groups (Medina & El-Sayed, 2009). Interestingly, controlled synthesis of PAMAM dendrimers provides a suitable nanocarrier for drug delivery. Typically, PAMAM dendrimers have a size of 2.3 nm in generation 2.0 (G 2.0) to 5.3 nm in G 5.0 (Svenson & Tomalia, 2012).

Importantly, PAMAM dendrimers have the size in the range of 1 to 10 nm, which can diffuse directly into tumor cells (Sinek et al., 2004). These formulations tend to accumulate in solid tumors via the enhanced permeability and retention (EPR) effect, thus avoiding accumulation in noncancerous tissues (Medina & El-Sayed, 2009).

Many chemotherapeutic drugs are derivatives of natural polyphenols or flavonoids. The major obstacles include their toxicity or poor bioavailability. Gallic acid (3,4,5-trihydroxy benzoic acid) is a natural polyhydroxy phenolic compound, generally found in various plants, fruits and foods (Kahkeshani et al., 2019). In recent past, GA has been shown chemopreventive and anti-proliferative activities against different types of human cancers (Verma et al., 2013). GA is known to have a broad spectrum of biological activities including antioxidant, anti-inflammatory, anti-microbial antiviral, anti-allergic, anti-melanogenic, and anti-mutagenic activities etc. (Badhani et al., 2015). Similar to other natural polyphenolic derivatives, GA also has poor bioavailability, limited tissue distribution and rapid degradation, which limit its clinical application to consider as drug candidate (Brglez Mojzer et al., 2016; Manach et al., 2005). In the recent past, GA was conjugated with PAMAM dendrimers and shown anti-proliferative response, but not explored the molecular mechanism of cell death (Sharma et al., 2011). In the present study, we chemically conjugated the GA with 4.0 G PAMAM dendrimers to extend the bioavailability and explored the molecular mechanism of inhibition of cell proliferation and induction of cell death in HCT116 cells.

Materials & methods

Materials

The molecular biology grade chemicals were purchased commercially. Gallic acid (GA), ethylenediamine (EDA), methyl acrylate (MA), 1-ethyl-3-(3-dimethylaminopropyl) carbodiimide hydrochloride (EDAC), Poly-L-lysine, (3-(4,5-dimethylthiazol-2-yl)-2,5-diphenyltetrazolium bromide (MTT), Trypan blue, 4',6-diamidino-2-phenylindole (DAPI), bicinchoninic acid (BCA) protein estimation kit, dialysis tubing cellulose membrane and anti-mouse horseradish peroxidase (HRP) conjugated secondary antibody were purchased from Sigma-Aldrich (St. Louis, MO, USA). RPMI-1640, DMEM, Dulbecco's Phosphate buffer saline (DPBS), Penicillin, Streptomycin, Neomycin (PSN) antibiotic cocktail, Fetal bovine serum (FBS), EnzChekCaspase-3 Assay Kit, Opti-MEM, Lipofectamine LTX, LysoTracker Red DND-99, Hoechst 33342 dye and antibody against cytochrome c, human IL1 β and IL-6 ELISA kits were purchased from Invitrogen (Life Technologies, USA). Annexin V-FITC/Propidium Iodide (PI) staining kit, 5,5',6,6'-tetrachloro-1,1',3,3'-tetraethylbenzimidazolylcarbocyanine iodide (JC-1) dye and Protein A-Sepharose beads were purchased from Biovision Inc. (California, USA). LDH cytotoxicity assay kit was purchased from Takara Bio Inc. (Shiga, Japan). The complete EDTA-free Protease inhibitor cocktail (PIC) was purchased from Roche Applied Science (Penzberg, Germany). 0.2 μ m PVDF membrane, iScript cDNA Synthesis Kit and ECL substrate were purchased from Bio-Rad (Philadelphia, USA). Antibodies against Bcl-

2, PARP, procaspase-9, procaspase-3, MMP-9, p53, p65, GAPDH, COX-IV, Histone H3, β -actin, and anti-rabbit HRP linked secondary antibodies were purchased from Cell Signaling Technology (Danvers, MA). Rabbit polyclonal antibody against Apaf-1 was purchased from BD Biosciences (New Jersey, USA). All other chemicals used were of analytical grade and purchased from Merck (Darmstadt, Germany).

Synthesis of 4.0 G PAMAM dendrimers

4.0 G EDA core PAMAM dendrimer was synthesized using Tomalia's divergent growth method (Tomalia et al., 1986). The Michael addition of primary amine (EDA in the first step) to the double bond of methyl acrylate (MA) resulted in the formation of ester terminated half-generation dendrimers, designated as G (*n* 0.5). This was followed by amidation of the carbomethoxy intermediate with a large excess of EDA in methanol to produce amine-terminated full generation dendrimers referred to as G (*n*). The reiteration of these two steps led to the formation of the next higher generation dendrimers. 4.0 G PAMAM dendrimer was synthesized using the above approach shown in Figure 1.

The Michael addition of EDA to methyl acrylate in methanol yields half-generation dendrimer denoted as G 0.5 whereas its further amidation with EDA in methanol yields a full generation dendrimer (G 1.0). The repetition of these two reactions yields a G 4.0 PAMAM dendrimer.

Synthesis of PAMAM-GA conjugate

The PAMAM-GA conjugate was synthesized by coupling reaction (Sharma et al., 2011). Gallic acid was covalently linked to 4.0 G PAMAM dendrimer using EDAC as a cross-linking agent. An aqueous solution of EDAC (2.24 mM) was mixed with ethanolic (1:1) solution of GA (2.24 mM) with constant stirring. Subsequently, 4.0 G PAMAM dendrimer (0.070 mM) was added dropwise with constant stirring in the dark. The stirring was continued for another 24 h at room temperature. Thereafter, the reaction mixture was placed for dialysis under distilled water to remove the byproducts and/or the unreacted reagents. The scheme of synthesis of PAMAM-GA conjugate has been shown in Figure 2.

Characterizations of PAMAM-GA conjugate

4.0 G of PAMAM dendrimer and PAMAM-GA conjugate were characterized by UV-Visible spectrophotometry, Fourier transform infrared spectroscopy (FT-IR) and ¹H NMR spectroscopy. Briefly, 0.01% (w/v) 4.0 G PAMAM dendrimer and PAMAM-GA conjugate were prepared in distilled water and scanned in the range of 200–400 nm using Multimode microplate reader (SpectraMax M2e, Molecular Devices, USA). Further, FT-IR Analysis was carried out by using Perkin Elmer, G-FTIR. Various peaks were interpreted for different groups. Surface group modification on dendrimer was studied through IR spectra. To confirm the synthesis of a conjugate, ¹H NMR spectra of 4.0 G PAMAM dendrimer and PAMAM-GA conjugate were recorded on Bruker Avance II (500 MHz) Bru

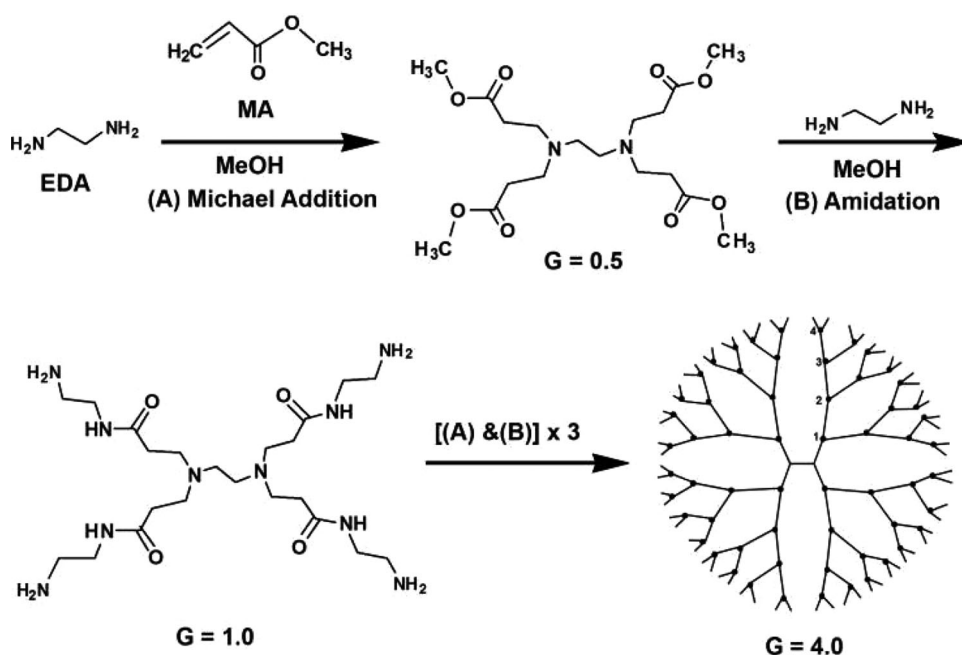


Figure 1. Schematic representation illustrating the synthesis of 4.0 G PAMAM dendrimer.

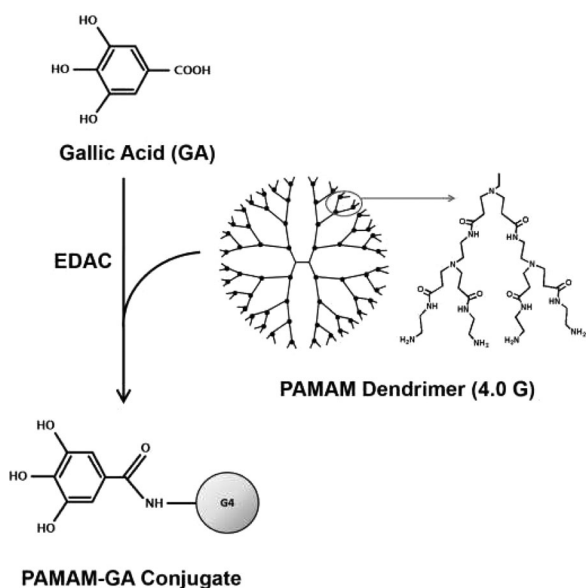


Figure 2. Scheme of the conjugation of GA with 4.0 G PAMAM dendrimer. GA was conjugated with PAMAM dendrimer using EDAC as a linker. This occurs via amide linkage between the $-\text{COOH}$ group of GA and surface $-\text{NH}_2$ group of PAMAM dendrimer.

spectrometer. The samples were solubilized in methanol. Chemical shifts were reported as δ (ppm) relative to Tetramethylsilane (TMS) as a standard. Various shifts in the peaks were interpreted for different groups present in the conjugated system. Moreover, the particle of the size of 4.0 G PAMAM dendrimer and PAMAM-GA conjugate was analyzed by Dynamic Light Scattering (DLS) particle size analyzer.

Cell lines and cell culture

The human colorectal carcinoma (HCT 116), human breast carcinoma (MCF7), human colorectal adenocarcinoma (HT29), and mouse embryonic fibroblast (NIH 3T3) cell lines were

obtained from National Centre for Cell Science (NCCS), Pune, India. HCT 116 and HT29 cells were maintained in RPMI-1640 and , MCF7, and NIH 3T3 cells were maintained in DMEM culture media, supplemented with 2 mmol/L L-Glutamine, 10% FBS and an antibiotic cocktail containing 5 mg/ml penicillin, 5 mg/ml streptomycin and 10 mg/ml neomycin (Gibco, Life Technologies, USA). The cells were maintained under humidified atmosphere with 5% CO_2 at 37 °C. Exponentially growing cells were used for all the experiments.

Treatment to cells with GA and PAMAM-GA conjugate

Stock solutions of PAMAM-GA conjugate was prepared in ultrapure RNase-free distilled water at a concentration of 100 mM and 60 mM respectively. The PAMAM-GA conjugate was filtered through a 0.2 μm sterilized filter before use. Exponentially cultured cells were treated with different concentrations of GA and PAMAM-GA conjugate (2.5 mM, 5 mM, and 10 mM) for mentioned time points in the figure legends.

Determination of IC_{50}

The IC_{50} of GA and PAMAM-GA conjugate was determined by MTT assay. Briefly, 1×10^4 HCT 116 and NIH 3T3 cells were seeded in a 96 well plate and incubated for 24 h. Cells were treated with GA (0–20 mM) and PAMAM-GA conjugate (0–20 mM) for 24 h. After completion of incubation, cells were washed using DPBS (pH 7.4) and 0.5 mg/ml of MTT solution was added to each well and allowed incubation for 4 h at 37 °C in a CO_2 incubator. Residual MTT was discarded and DMSO was added to dissolve the formazan crystals. Absorbance was recorded at a wavelength of 570 nm with a reference of 650 nm using a Multimode microplate reader (SpectraMax M2e, Molecular Devices, USA). The results were represented in terms of percentage inhibition of cell

proliferation and IC_{50} values were determined from the dose-response curve using Sigma Plot 12.0.

Cell proliferation and cell viability assay

The effect of GA and PAMAM-GA conjugate on cell proliferation was evaluated by MTT assay as described above. Subsequently, cell viability was carried out by trypan blue exclusion assay. HCT 116, HT 29, MCF 7 and NIH 3T3 cells were treated with 2.5 mM, 5 mM and 10 mM of GA and PAMAM-GA conjugate for 6 h, 12 h, and 24 h respectively. Cells were harvested, washed and resuspended in DPBS (pH 7.4). The cell suspension was mixed with an equal amount of 0.4% trypan blue solution and allowed to incubate for 2–3 min. Live and dead cells were counted and the percentage of cell viability was calculated using formula, % cell death = Number of dead cells/Total number of cells \times 100. The results are represented in terms of the percentage of cell death relative to untreated control.

In vitro release and cellular uptake assay

In vitro release of Gallic acid (GA) from PAMAM-GA conjugate was monitored by the dialysis method. A known quantity (1.0 mg/ml) of GA and PAMAM-GA conjugate were filled in a dialysis tube (10 kDa). The dialysis tube was suspended in 10 ml of RPMI-1640 medium supplemented with 10% FBS and 1% PSN. The entire system was maintained at 37 ± 0.5 °C at the constant stirring of 200 ± 2 rpm. 1 ml of the medium was withdrawn at respective time points and replaced with fresh media. The absorbance of GA was recorded at 227 nm using a Multimode microplate reader (SpectraMax M2e, Molecular Devices, USA). Further, the concentration of drug release was quantified using the standard curve of GA. In addition, cellular uptake of PAMAM-GA conjugate in the cells was examined by detecting the presence of GA in the cell lysate. In brief, 1×10^5 HCT-116 cells were seeded in a 24 well plate and allowed to grow for 24 h. Thereafter, the cells were treated with different concentrations of PAMAM-GA conjugate for 6 h and 12 h. The cells were washed with DPBS (pH 7.4) twice and lysed with 0.1% Triton-X 100 (in DPBS). GA concentration in supernatants was measured at a wavelength of 290 nm using a Multimode microplate reader (SpectraMax M2e, Molecular Devices, USA). Cellular accumulation of GA was normalized to total protein content. The protein concentration was determined by using a BCA protein assay kit (Sigma-Aldrich, USA) according to the manufacturer's instructions.

Clonogenic ability assay

The *in vitro* cell survival assay was performed to examine the effect of PAMAM-GA conjugate on colony-forming ability of HCT 116 cells. Briefly, 4×10^4 cells were seeded in a 48-well plate. Cells were treated with 2.5 mM, 5 mM and 10 mM of PAMAM-GA conjugate for 6, 12 and 24 h. After completion of incubation, cells were trypsinized and 1,000 viable cells were seeded in a 6-well plate. The cells were allowed to grow

RPMI 1640 complete cell culture medium for 8–10 days for colony formation. The visible colonies were fixed with methanol and stained with 0.2% crystal violet stain. The data were represented as percentage plating efficiency (PE), defined as % PE = (Number of colonies formed/Number of cells seeded) \times 100.

Wound healing assay

The effect of PAMAM-GA conjugate on cell migration was monitored by *in vitro* wound-healing assay as described earlier (Vaidya et al., 2019). Briefly, 5×10^5 HCT 116 cells were seeded in a 6 well plate and allowed to reach confluency. A scratch was created in the confluent monolayer using a sterile tip. The cells were washed with DPBS to remove debris and subsequently, treated with different concentrations of PAMAM-GA conjugate in a serum-free medium as described in the figure legend. After completion of incubation, the medium was replaced with fresh serum-free medium and cells were allowed to migrate for 72 h. The images of scratches were captured under the DIC filter of the inverted microscope (DP71, Olympus, Japan). The distance covered by the migrating cells was calculated by comparing the same field at 0 h and 72 h using Image-Pro MC 6.1 (Bethesda, MD, USA).

Analysis of apoptotic cell death

The apoptotic potential of PAMAM-GA conjugate was examined by Annexin V/PI staining using Annexin V-FITC/PI apoptosis assay kit (Biovision Inc, California) as described previously (Vaidya et al., 2019). More than 100 cells from random fields were examined for apoptotic cell death. All the images were acquired by fluorescence inverted microscope using Image-Pro MC 6.1 software (Bethesda, MD, USA) and analyzed by Image J software (NIH, USA). Further, to confirm changes in mitochondrial membrane potential (MMP) was monitored by using a lipophilic fluorescent probe JC-1. For qualitative analysis, cells were treated with 2.5 mM, 5 mM and 10 mM of PAMAM-GA conjugate for different time points mentioned in the figure legend. Thereafter, cells were stained with JC-1 dye (5 μ g/ml) for 20 min in dark at 37 °C. Subsequently, the cells were counterstained with DAPI for 5–7 min in dark at room temperature and observed under a fluorescent microscope (DP-71, IX81, Olympus, Japan). More than 100 cells from three random fields were examined for the change in MMP. All the images were acquired by Image-Pro MC 6.1 (Bethesda, MD, USA) and analyzed by Image J software (NIH, USA). In addition, for quantitative analysis, the treated cells were stained with JC-1 dye (5 μ g/ml) for 20 min in the dark at 37 °C. Subsequently, the fluorescence was quantified using a Multimode microplate reader at the excitation of 485 nm and the emission at 527 nm (green fluorescence) and 590 nm (red fluorescence). The ratio of red fluorescence to green fluorescence was considered as a change in the Mitochondrial Membrane Potential ($\Delta\Psi_m$).

Caspase-3 activity assay

The activity of caspase-3 was examined by using the EnzChek Caspase-3 Assay Kit (Invitrogen, Life Technologies, USA) according to the manufacturer's protocol. Briefly, 1×10^6 HCT 116 cells were treated with 2.5 mM, 5 mM and 10 mM of PAMAM-GA conjugate for different time points as shown in the figure legend. Untreated cells were used as control. After completion of incubation, cells were harvested and washed twice with DPBS. The pellet was resuspended in 1X cell lysis buffer for 30 min and centrifuged at 5000 rpm for 5 min at 4 °C. The amount of protein in the resultant supernatant was estimated using the BCA protein estimation kit. The 100 µg protein was mixed with a 2X substrate solution containing 50 µM Z-DEVD-R110 substrate and incubated at room temperature for 30 min in the dark. The fluorescence was measured at an excitation and emission wavelength of 496 nm and 520 nm respectively using multimode plate reader (SpectraMax M2e, Molecular Devices, USA).

Necrotic cell death assay

The Necrotic cell death (cytotoxic effect) of GA and PAMAM-GA conjugate was examined by release of LDH using LDH activity assay kit (Takara Bio Inc., Shiga, Japan) according to the manufacturer's instruction. Briefly, HCT 116 cells and NIH 3T3 cells were treated with 2.5 mM, 5 mM and 10 mM of PAMAM-GA conjugate for 6, 12 and 24 h. The assay was performed as mentioned previously (Ranjan & Pathak, 2016). Microscopic assessment of cytotoxicity was carried out using Hoechst and propidium iodide staining as described previously (Vaidya et al., 2019). Cells were analyzed under a fluorescence inverted microscope (DP71, Olympus, Japan) and images were analyzed using ImageJ software (NIH, Bethesda). Hoechst-stained nuclei were counted and judged as either viable (lack of propidium iodide staining), apoptotic (Hoechst-stained condensed nuclei with propidium iodide-stained spots), or necrotic (large nuclei intensely stained with Hoechst and propidium iodide-stained).

Lysosomal integrity assay

The effect of GA and PAMAM-GA conjugate on lysosomal membrane integrity was examined by using LysoTracker Red DND-99 dye (Invitrogen, Life Technologies, USA). HCT 116 cells were treated with GA and PAMAM-GA conjugate shown in the figure legend and further stained with LysoTracker red for 1 h at 37 °C, followed by counterstaining with DAPI (1 µg/ml) for 5–7 min in the dark. More than 100 cells from random fields were examined under a fluorescence inverted microscope (DP-71, IX81, Olympus, Japan). All the images were acquired by Image-Pro MC 6.1 (Bethesda, MD, USA) and analyzed by Image J (NIH, USA).

Sub-cellular fractionation and western blotting

The expression of cell death regulatory proteins was examined from mitochondrial and cytosolic fractions as described earlier

(Waghela et al., 2015). In brief, After completion of treatment, cells were harvested and lysed in lysis buffer containing 250 mM sucrose, 70 mM KCl, 137 mM NaCl, 4.3 mM Na_2HPO_4 , 1.4 mM KH_2PO_4 , 100 µM PMSF and 1X protease inhibitor cocktail (Roche, Germany) for 5 min on ice. The lysate was centrifuged at $1,000 \times g$ for 5 min at 4 °C and the resulting supernatant was collected as the cytosolic fraction. The pellet was resuspended in mitochondrial lysis buffer containing 50 mM Tris-HCl (pH 7.4), 150 mM NaCl, 2 mM EDTA, 2 mM EGTA, 0.2% (v/v) Triton X-100, 0.3% NP-40, 100 µM PMSF and 1X protease inhibitor cocktail for 5 min on the ice. Pellet was disrupted in cell disruptor and centrifuged at $10,000 \times g$ for 5 min at 4 °C and the supernatant was collected as a mitochondrial fraction to examine the expression of cytochrome c and COX-IV. The whole cell lysate was prepared using RIPA buffer containing a protease inhibitor cocktail (Roche, USA). Cells were kept on the ice for 30 min followed by disruption and centrifugation at 8,000 rpm for 10 min at 4 °C and supernatant was collected. For collection of nuclear fractions, cells were lysed in hypotonic buffer (10 mM HEPES-K⁺ pH 7.5, 10 mM KCl, 1.5 mM MgCl_2 , 0.1 mM DTT, 0.5% Triton X-100, 1 mM PMSF and 1x PIC) for 5 min on ice and spun at 3000 rpm for 2 min at 4 °C. The pellets were washed with wash buffer (10 mM HEPES-K⁺ pH 7.5, 10 mM KCl, 1.5 mM MgCl_2 , 0.1 mM DTT, 1 mM PMSF and 1x PIC) and subsequently lysed with lysis buffer (150 mM NaCl, 1% Triton X-100, 0.5% Sodium deoxycholate, 0.1% SDS, 50 mM Tris pH 8.0, 1 mM PMSF, 1 mM NaV and 1x PIC) for 25 min on ice and spun at 10,000 rpm for 15 min. The supernatant was collected as nuclear fraction. Protein concentration was determined by using a BCA protein estimation kit (Sigma-Aldrich, USA) according to the manufacturer's protocol. 50 µg protein was resolved on 10% SDS-PAGE and transferred to PVDF membrane by wet electro-blotting method at 4 °C. The membrane was blocked with 5% non-fat milk in TBST (10 mM Tris-HCl (pH 7.4), 0.9% NaCl and 0.05% Tween 20) for 4 h at room temperature followed by overnight incubation with primary antibody against p65 (1:1000), cytochrome c (1:1000), procaspase-3 (1:1000), PARP (1:1000), Bcl-2 (1:250), MMP-9 (1:250), Histone H3 (1:1000), COX-IV (1:1000), β -actin (1:10,000) and GAPDH (1:1000) at 4 °C. After washing with TBST, the membrane was probed with HRP conjugated secondary antibodies (1:10,000). Expression of immune reactive protein was detected by using Clarity Western ECL substrate kit according to the manufacturer's instruction and developed on Kodak X-Omat blue film (NEN Life Sciences, Inc., Boston, MA) in the dark.

Co-immunoprecipitation assay

To analyze the formation of the apoptosome complex, a co-immunoprecipitation assay was carried out as described earlier (Ranjan & Pathak, 2016). In brief, 1×10^6 HCT 116 cells were seeded in 60 mm dishes and treated with PAMAM-GA conjugate for 12 h. The cells were lysed using lysis buffer (20 mM Tris-Cl (pH 7.4), 150 mM NaCl, 10% glycerol, 1% Triton-X-100) containing 1X protease inhibitor cocktail (Roche, USA) for 30 min at 4 °C, followed by disruption and centrifugation at $15,000 \times g$ for 15 min at 4 °C. The clarified supernatant was collected and its protein concentration was

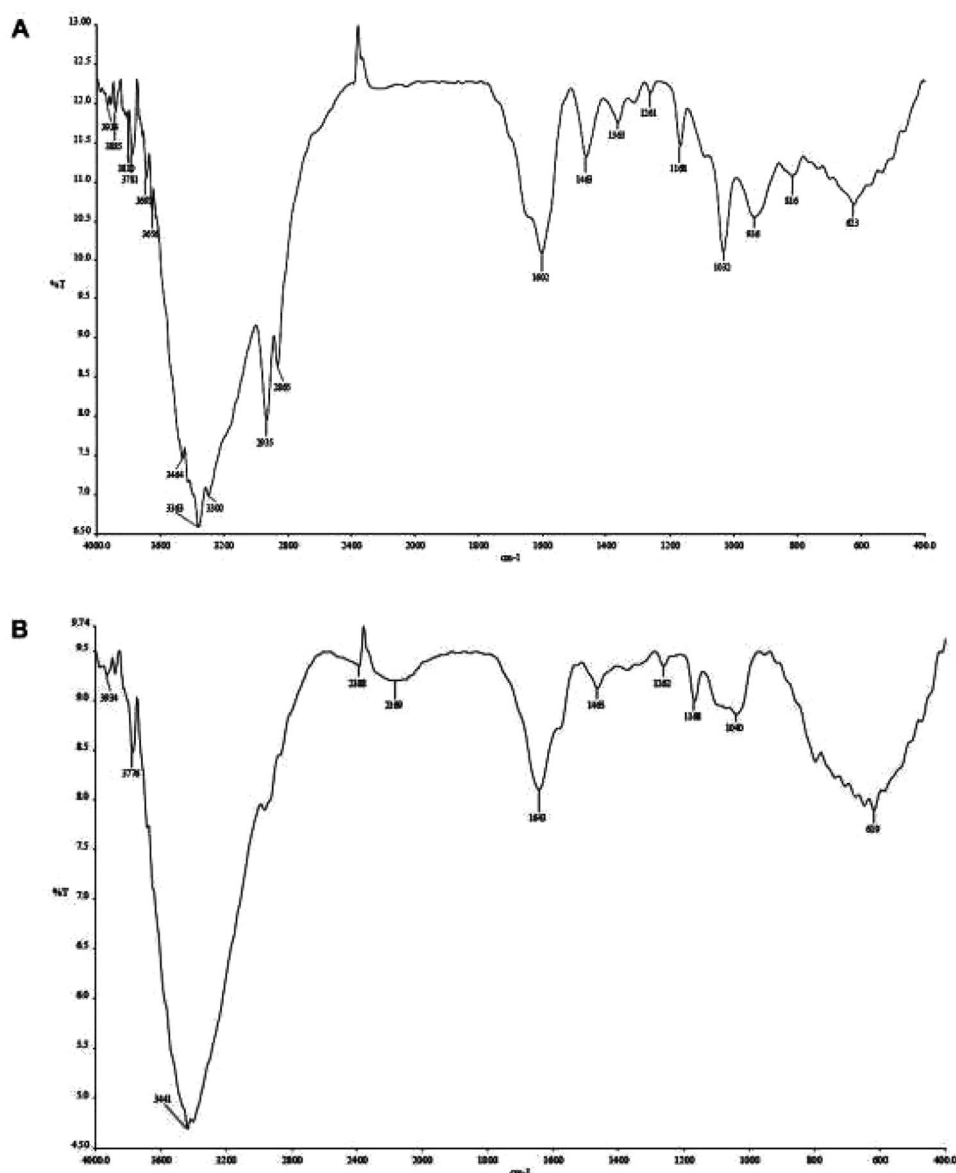


Figure 3. Characterization of PAMAM-GA conjugate by FT-IR Spectroscopy. FT-IR spectra of (A) 4.0 G PAMAM dendrimer (B) PAMAM-GA conjugate.

estimated using the BCA protein estimation kit (Sigma-Aldrich, USA) according to the manufacturer's protocol. 200 μ g of protein was incubated with 20 μ l Protein A-Sepharose beads (BioVision, USA) for 1 h at 4 $^{\circ}$ C with gentle shaking. The mixture was centrifuged at 3000 rpm for 5 min at 4 $^{\circ}$ C and the supernatant was further incubated with 1 μ g anti-Apaf-1 antibody and 20 μ l Protein A-Sepharose beads at 4 $^{\circ}$ C with gentle shaking for overnight. The immunoprecipitated complexes were washed thrice with RIPA buffer, denatured in 6X Laemmli sample buffer and subjected to immunoblotting using the antibody against pro-caspase-9 (1:1000), cytochrome-c (1:500) and Apaf-1 (1:250) as described above.

p65 translocation assay

To examine the NF- κ B activation the translocation of p65 from cytoplasm to nucleus was monitored using fluorescent microscope as described earlier (Vaidya et al., 2019). In brief,

HCT 116 cells were transfected with pEGFP-p65 (gifted by Dr. Johannes Schmid, Med. Uni. Vienna) using Lipofectamine LTX with Plus reagent (Life Technologies, USA). 24 h post-transfection, the cells were treated with 2.5 mM, 5 mM and 10 mM PAMAM-GA conjugate for 6 h followed by treatment of TNF- α for 1 h. Thereafter, the cells were washed with DPBS and analyzed under fluorescence inverted microscope. Untreated cells were used as control. More than 100 cells from random fields were examined for translocation of GFP tagged p65 from cytosol to nucleus. All the images were acquired under inverted microscope (DP71, Olympus Japan) using Image-Pro MC 6.1 software (Bethesda, MD, USA) and analyzed by Image J software (NIH, USA).

Quantitative gene expression by real-time PCR

The mRNA expression of IL-1 β and IL-6 was analyzed in HCT116 cells upon treatment of PAMAM-GA conjugate for 24 h followed by exposure of TNF- α (10 ng/mL) for 1 h. Total

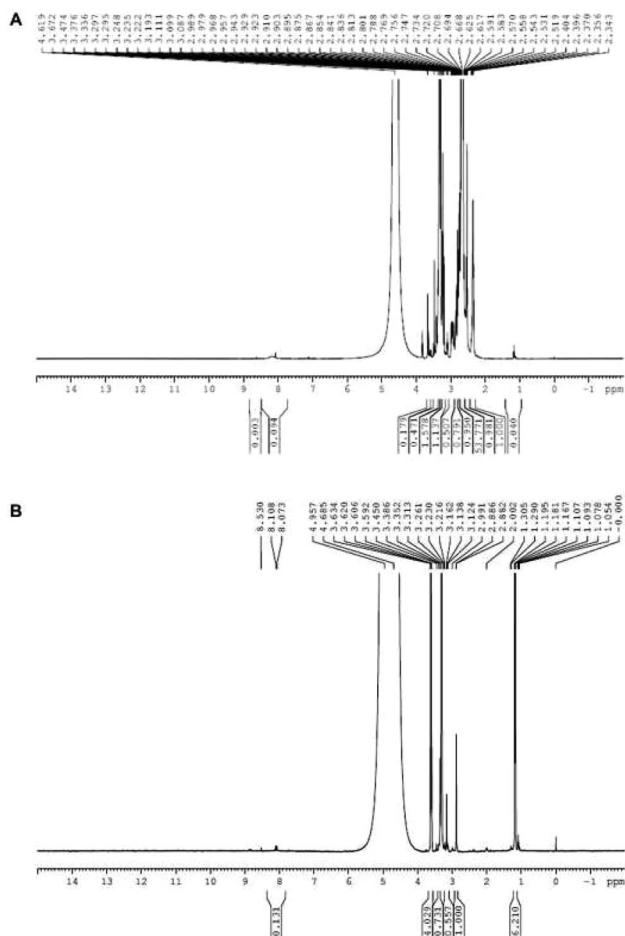


Figure 4. Characterization of PAMAM-GA conjugate by NMR. ^1H NMR spectra of (A) 4.0G PAMAM dendrimer (B) PAMAM-GA conjugate.

RNA was isolated with Trizol reagent (Invitrogen, UK) according to manufacturer's protocol. The concentration of total RNA was determined by taking the absorbance at 260/280 nm under UV-visible spectrophotometer (PG Instrument, USA, T90); 1 μg of total RNA was reversely transcribed, and cDNA was synthesized using iScript cDNA Synthesis Kit (Bio-Rad Laboratories Inc., Hercules, CA, USA). A real-time PCR was performed using the StepOne plus real-time PCR detection system (Applied Biosystems, Carlsbad, California). The reaction was conducted with 20 μL final reaction volume containing 0.2 μL (100 pMolar) of cDNA, 10 μL iQTM SYBR[®] Green Supermix (Bio-Rad, USA), and 2 μL (1 μM) of each primer and remaining 5.8 μL of nuclease free water. All reactions were performed in MicroAmp fast optical 96well PCR plates (Applied Biosystem) and sealed with optical adhesive covers (Applied Biosystem). 18SrRNA was used as the endogenous control. Thermal cycler conditions were as follows: After denaturing at 95°C for 10 min, PCR was performed for 40 cycles, each of which consisted of denaturing at 95°C for 15 s, annealing/extending at 65°C for 1 min. Afterwards, final PCR products were heated to 72°C for 30 s, and the expected size products were confirmed by melting curve analysis. These following sets of PCR primers were used. IL-1 β forward, 5'-GACAACGAGCGTACGTTCA-3' and reverse, 5'-CGATTCTGTTGACTATCCCGTAA-3', IL-6 forward, 5'-GCTGC

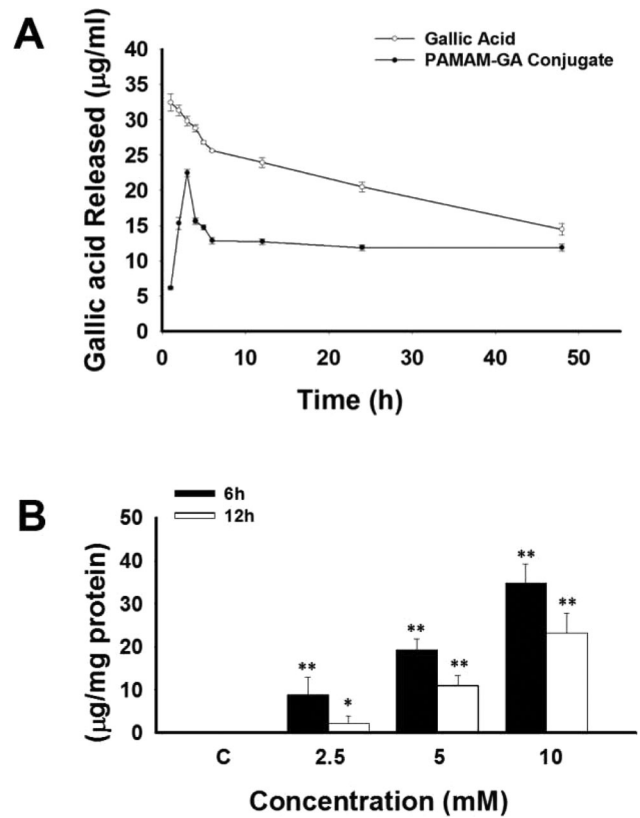


Figure 5. Release of GA from PAMAM-GA conjugate & uptake. (A) A known quantity (1 mg/ml) of GA and PAMAM-GA conjugate was placed in a dialysis tube and suspended in RPMI 1640 medium with 10% FBS at 37°C. At mentioned time points, 1 ml of medium was withdrawn and the absorbance of GA was measured at 430 nm. The released amount of GA was quantified using its standard curve. The plot represents the amount of GA released at mentioned time points. (B) HCT 116 cells treated with PAMAM-GA conjugate for 6 h and 12 h, were harvested and lysed with 0.1% Triton-X100. The absorbance of GA was recorded in cell lysate at 290 nm using a Multimode microplate reader. The graphs represent intracellular concentration of GA against the concentration of PAMAM-GA conjugate. Error bars represent mean \pm SEM of three independent experiments. The difference is significant between GA and PAMAM-GA treatment groups at * $p \leq 0.05$, ** $p \leq 0.01$ and *** $p \leq 0.001$.

AGGCACAGAACCA-3' and reverse, 5'-ACTCCTTAA AGCTGCGC AGAA-3', 18S rRNA Forward, 5'-AGAAACGGCTA CCAC ATCCAA-3' and reverse, 5'-TGTCACTACCTCCCCGTGTCA-3'. Each assay was normalized by using the difference in critical thresholds between target genes and 18SrRNA.

ELISA (enzyme-linked immunosorbent assay)

To examine the release of pro-inflammatory cytokines, ELISA was carried out. 1×10^5 HCT116 cells were treated with PAMAM-GA conjugate for 24 h followed by exposure of TNF- α (10 ng/mL) for 1 h. The media was collected, and the ELISA was performed. ELISA plate was coated with 100 μL /well of captured antibody in Coating buffer and the plate was sealed and incubated overnight at 4°C. Next, buffer was aspirated from each well and washed 3 times with 250 μL /well wash buffer for 1 min each. The surface of wells were blocked with 200 μL /well of 1x assay diluent solution and incubated at room temperature for 1 h. 100 μL /well of the sample was added to the appropriate well and plate was sealed and incubated at room temperature for 2 h. Subsequently, each well was washed with wash buffer and

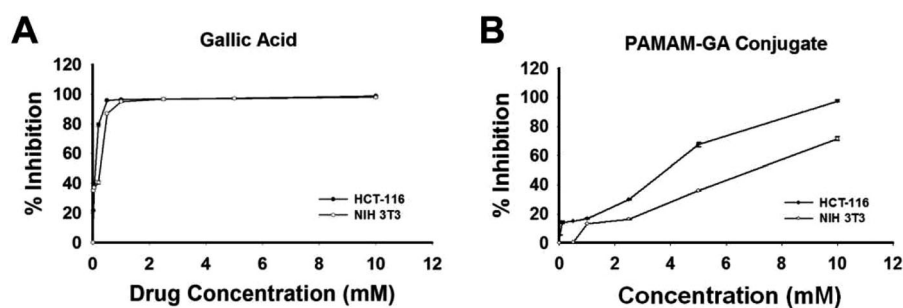


Figure 6. Effect of GA and PAMAM-GA conjugate on cell proliferation. IC₅₀ values of (A) GA and (B) PAMAM-GA conjugate on HCT-116 and NIH-3T3 cells by MTT assay. Cells were treated with a series of concentrations of GA or PAMAM-GA conjugate for 24 h and MTT assay was carried out to determine the inhibition in cell proliferation. IC₅₀ values were calculated from the dose-response curve using SigmaPlot 13.0

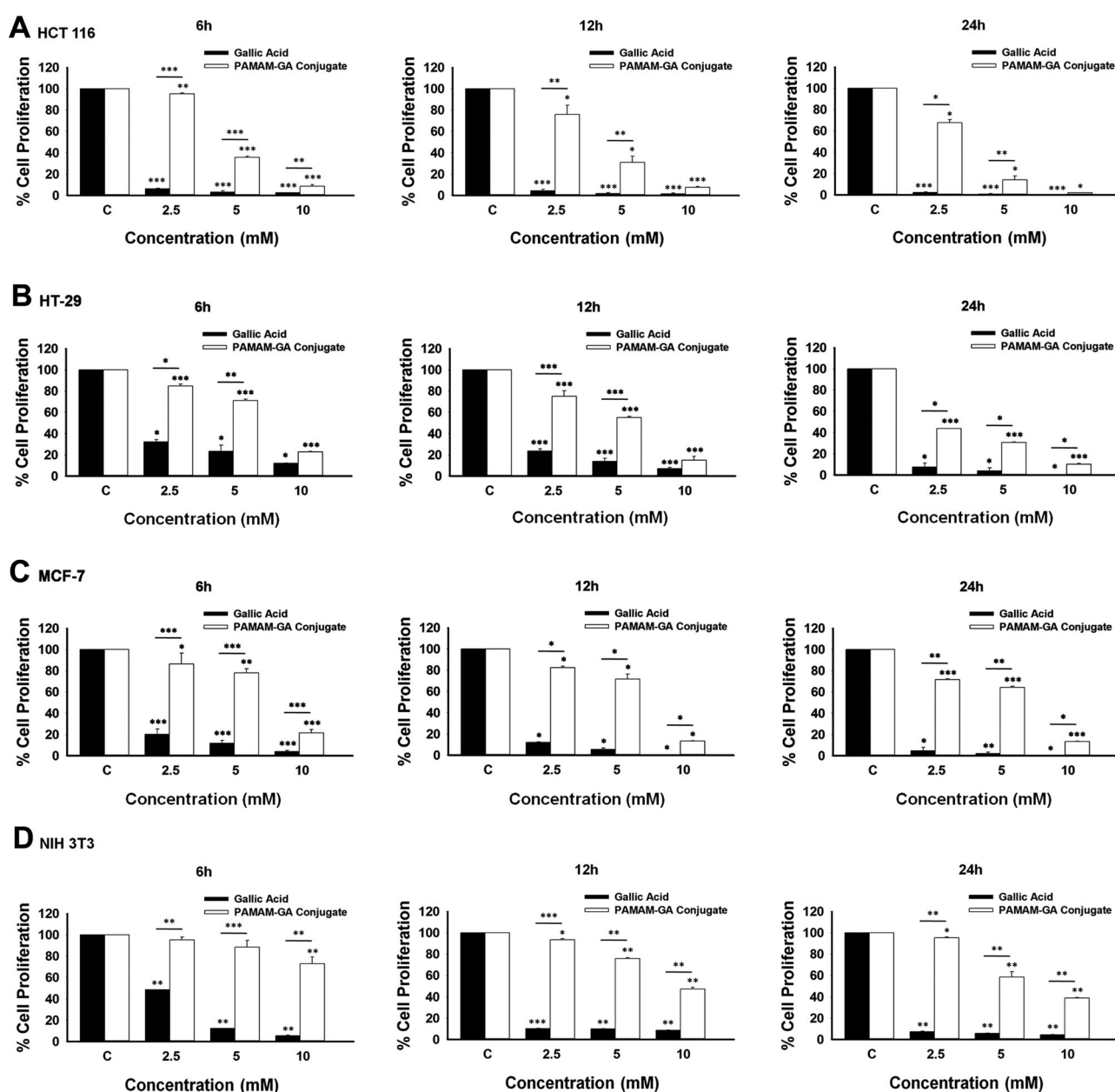


Figure 7. Effect of GA and PAMAM-GA conjugate on cell proliferation. (A) HCT 116, (B) HT-29, (C) MCF-7, and (D) NIH 3T3 cells were treated with 2.5 mM, 5 mM and 10 mM GA and PAMAM-GA conjugate and MTT assay was carried out to determine their effect on cell proliferation. Error bars represent mean \pm SEM of three independent experiments. The difference is significant between GA and PAMAM-GA treatment groups at * $p \leq 0.05$, ** $p \leq 0.01$ and *** $p \leq 0.001$.

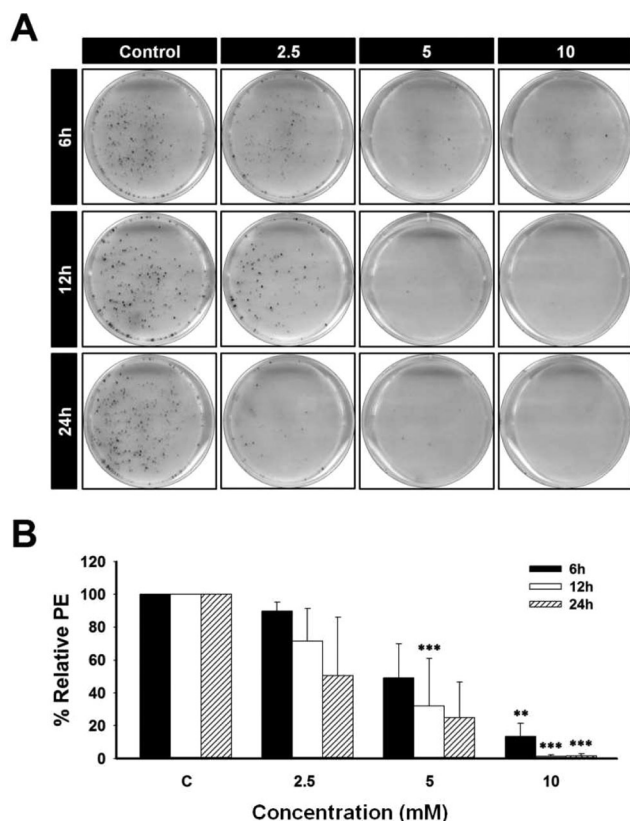


Figure 8. Effect of PAMAM-GA conjugate on cell survival. The effect of PAMAM-GA conjugate on cell survival was monitored by colony formation assay. HCT 116 cells were treated with indicated concentrations of PAMAM-GA conjugate for 6 h, 12 h, and 24 h. Subsequently, the cells were harvested, 1000 viable cells were seeded in a 6 well plate and allowed to grow for 8–10 days. The colonies were fixed with methanol and stained with crystal violet. The colonies were counted and plating efficiency was determined from it. (A) Representative images of the colonies formed. (B) The graph represents the relative plating efficiency of the cells at indicated time points and the concentration of PAMAM-GA conjugate treatment. Error bars represent mean \pm SEM of three independent experiments. * $p \leq 0.05$, ** $p \leq 0.01$ and *** $p \leq 0.001$ compared to untreated control cells.

after that 100 μ L/well detection antibody was added. The plate was sealed and incubates at room temperature for one hour followed by repeated washing. 100 μ L/well of Avidin-HRP was added and plate was sealed and incubated at room temperature for 30 min followed by repeated washing. 100 μ L/well of substrate solution was added to each well and the plate was incubated at room temperature for 15 min. Finally, 50 μ L/well of stop solution was added to each well and absorbance was recorded at a wavelength of 450 nm and 570 nm respectively. The value of absorbance of 570 nm was subtracted from the absorbance of 450 nm for further analysis. The concentration of secreted IL-6 and IL-1 β was determined from its standard curve.

Statistical analysis

Data were analyzed by one-way analysis of variance (ANOVA) followed by Student Newman Keuls (SNK) test for multiple comparisons using Sigma Plot 13.0 statistical analysis software. The data were tested for normality by the Shapiro-Wilk test prior to ANOVA. Values were expressed as mean \pm SEM from three independent experiments. For the experiments involving only two groups, a Student t-test was used.

Differences were considered statistically significant at * $p \leq 0.05$, ** $p \leq 0.01$, *** $p \leq 0.001$.

Results

Characterization of 4.0G PAMAM dendrimer and PAMAM-GA conjugate

Gallic acid was conjugated with 4.0G PAMAM dendrimer shown in the schematic representation (Figure 2). The conjugation was confirmed by UV-Vis spectroscopy, FT-IR spectral analysis, NMR spectroscopy, and particle size analysis. The λ_{max} of 4.0G PAMAM dendrimer was recorded at 300 nm, whereas λ_{max} of PAMAM-GA conjugate was shifted to 290 nm that was examined by UV-Vis spectroscopy (Figure S1). Further, FT-IR analysis revealed the appearance of the peak of the amide linkage at 1643 cm^{-1} and aromatic linkage (C=C) at 1465 cm^{-1} that denotes the conjugation of 4.0G PAMAM dendrimer with GA (Figure 3). The NMR spectra also revealed the formation of PAMAM-GA conjugate with significant changes in integral values and shifts of the secondary $-\text{CH}_2$ group that was observed upon conjugation. The important shifts obtained in NMR spectra that were for; 4.0G PAMAM Dendrimer: ^1H NMR (MeOD) δ 2.54 ($-\text{NCH}_2\text{CH}_2\text{N}-$); δ 2.53 ($-\text{NCH}_2\text{CH}_2\text{CO}-$); δ 2.37 ($-\text{NCH}_2\text{CH}_2\text{CO}-$); δ 3.29 ($-\text{CONHCH}_2\text{CH}_2\text{N}-$); δ 2.55 ($-\text{CONHCH}_2\text{CH}_2\text{N}-$); δ 3.47 ($-\text{CONHCH}_2\text{CH}_2\text{NH}_2$); δ 2.57 ($-\text{CONHCH}_2\text{CH}_2\text{NH}_2$); 4.0G PAMAM- GA conjugate: ^1H NMR (MeOD) δ 3.13 ($-\text{NCH}_2\text{CH}_2\text{N}-$); δ 3.31 ($-\text{NCH}_2\text{CH}_2\text{CO}-$); δ 2.88 ($-\text{NCH}_2\text{CH}_2\text{CO}-$); δ 3.59 ($-\text{CONHCH}_2\text{CH}_2\text{N}-$); δ 3.45 ($-\text{CONHCH}_2\text{CH}_2\text{N}-$); δ 8.53 ($-\text{NHCO-GA}$); δ 8.07–8.10 (Ar-H). The appearance of newer peaks of amide linkage [$-\text{NHCO-GA}$] at 8.53 ppm and Ar-H at 8.07–8.10 ppm, confirms the formation of PAMAM-GA conjugate (Figure 4). PAMAM dendrimer and PAMAM-GA conjugate were further subjected to analysis of particle size distribution. The particle size of 4.0G PAMAM dendrimer and PAMAM-GA conjugate was found \sim 5.2 nm. However, the conjugation of GA with PAMAM dendrimer did not show a major alteration in the particle size. Minor changes in effective diameter were observed. The average effective diameter of PAMAM dendrimer and PAMAM-GA conjugate was obtained as 198.0 and 211.7 nm respectively (Figure S2).

PAMAM-GA conjugate exhibits sustained release and cellular uptake of GA from PAMAM-GA conjugate

We examined the release study of Gallic acid from PAMAM-GA conjugate *in vitro* at various time points. We found that PAMAM-GA conjugate exhibits slow release than the free Gallic acid (Figure 5(A)). Thus, the results illustrate that conjugation of Gallic acid with PAMAM dendrimer shows improved stability and sustained release that may enhance permeable retention effects and cellular uptake. Further, the uptake of GA from PAMAM-GA conjugate on HCT 116 was examined. The results showed that the amount of GA in the cell increased in a dose-dependent manner at 6 h. The highest amount of GA concentration was found on the cells treated with 10 mM PAMAM-GA conjugate at 6 h as compared to other

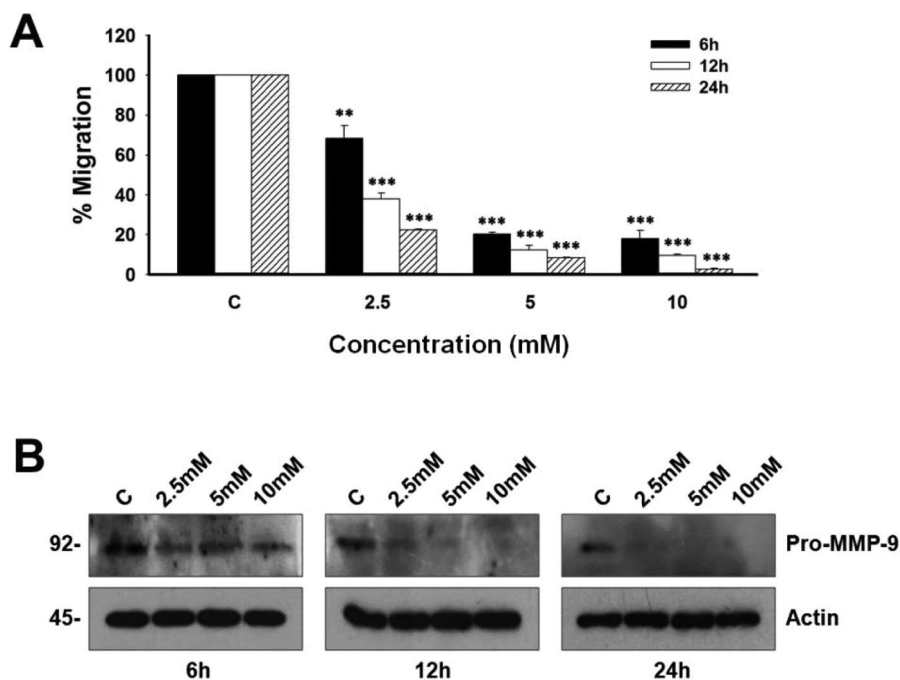


Figure 9. Effect of PAMAM-GA conjugate on cell migration. The migration ability of HCT 116 cells was determined by wound scratch assay and western blotting after treating the cells with mentioned concentrations of PAMAM-GA conjugate for 6 h, 12 h, and 24 h. (A) The graph represents the % migration of the cells. (B) PAMAM-GA conjugated treated HCT 116 cells were harvested for analyzing the expression of Pro-MMP-9. β -actin was used as a loading control. Error bars represent mean \pm SEM of three independent experiments. * $p \leq 0.05$, ** $p \leq 0.01$ and *** $p \leq 0.001$ compared to untreated control cells.

concentrations (Figure 5(B)). This result indicates that PAMAM-GA conjugate gets internalized inside the cells within 6 h.

Determination of IC_{50} of GA and PAMAM-GA conjugate

The half-maximal inhibitory concentration (IC_{50}) of GA and PAMAM-GA conjugate was determined from the dose-response curve on HCT 116 and NIH 3T3 cells. These cells were treated with different concentrations of GA and PAMAM-GA conjugate for 24 h. The IC_{50} value for GA and PAMAM-GA conjugate was found 69 μ M and 3.68 mM respectively in HCT 116 cells. On the other hand, the IC_{50} value for NIH 3T3 cells was found 260 μ M with the treatment of GA and 6.5 mM with the treatment of PAMAM-GA conjugate. Indeed, IC_{50} of PAMAM-GA conjugate was significantly higher in NIH 3T3 as compared to the HCT 116 cells (Figure 6). These results indicate that PAMAM-GA is effective at low concentration to cancer cells and less toxic to normal NIH 3T3 cells. Moreover, GA showing inhibition in cell proliferation at lower concentration in HCT 116 and NIH 3T3 cells, but the conjugation of GA with PAMAM dendrimers was showing more efficacious and promising response as compared to free GA. Thus, these results demonstrate that conjugation with PAMAM dendrimer reduces the toxicity of GA.

PAMAM-GA conjugate inhibits cell proliferation specifically in cancer cells

We examined the anti-proliferative effect of PAMAM-GA conjugate on the different origins of cancer cells (HCT-116, HT-29, MCF-7) using MTT assay. The results show that PAMAM-GA conjugate significantly inhibits cell proliferation of HCT-116, HT-29 and MCF-7 (Figure 7). Although, free GA was found to induce

excessive cell death at a lower concentration in both HCT 116 and NIH 3T3 cells, whereas PAMAM-GA conjugate showed significant cell death to cancer origin cells, but not to the normal NIH 3T3 cells (Figure S3). We found, similar response on cell death examined by trypan blue exclusion assay in HCT-116 cell (Figure S3). Next, we examined the effect of PAMAM-GA conjugate on cell survival by examination of the clonogenic ability of the cells. The results showed that PAMAM-GA conjugate inhibits colony formation in a dose and time-dependent manner on HCT-116 cells (Figure 8(A, B)).

PAMAM-GA conjugate inhibits cell migration and downregulates MMP-9 expression

The effect of PAMAM-GA conjugate on cellular migration was analyzed by wound healing assay and expression of MMP-9, which is associated with cell migration and invasiveness. We found that PAMAM-GA conjugate profoundly inhibits the migration of HCT 116 cells in a dose and time-dependent manner as compared to the control (Figure 9(A)). Cell migration is associated with upregulated expression of matrix metalloproteinases. The result show HCT116 cells treated with PAMAM-GA conjugate downregulating the expression of Pro form of MMP-9 (Figure 9(A, B)). The results suggest that PAMAM-GA conjugate inhibits colony formation and migration ability of HCT 116 cells for cell survival.

PAMAM-GA conjugate induces cell death via activating apoptosis signaling

PAMAM-GA conjugate inhibits cell proliferation of cancer cells. Therefore, it was important to unravel the molecular

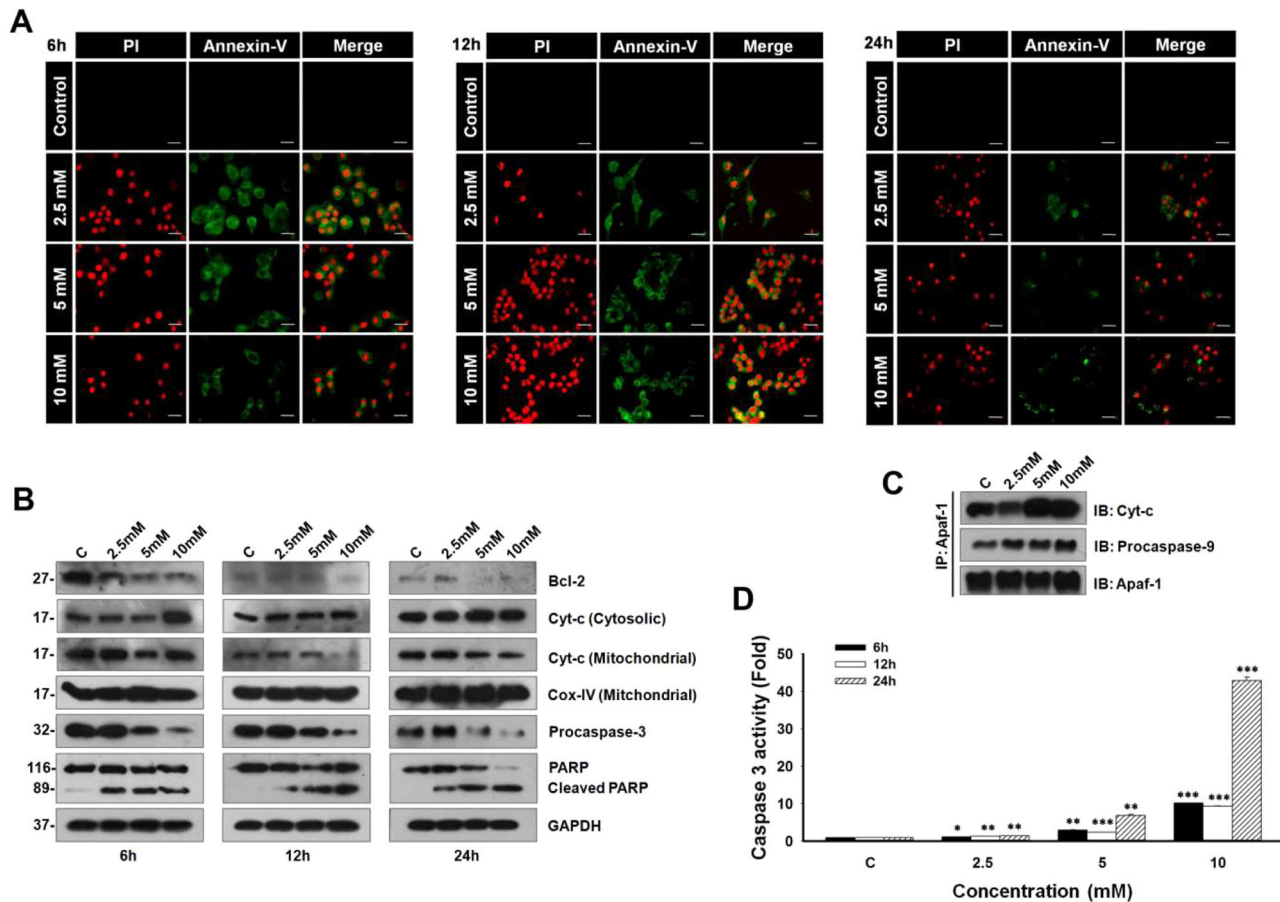


Figure 10. PAMAM-GA conjugate induces apoptotic cell death. (A) HCT 116 cells were treated with mentioned concentrations of PAMAM-GA conjugate for 6 h, 12 h, and 24 h, followed by staining with Annexin V-FITC and PI. The cells were analyzed using a fluorescence microscope. Scale bar: 10 μ m. (B) After treating with mentioned concentrations of PAMAM-GA conjugate for the indicated time, HCT 116 cells were harvested for analyzing the expression of Bcl-2, Procaspase-3, and PARP cleavage. To monitor the release of cytochrome c from mitochondria to cytosol, the PAMAM-GA conjugate treated cells were subjected to subcellular fractionation, followed by western blotting for cytochrome c. GAPDH and COX-IV represent loading control. (C) HCT 116 cells were treated with mentioned concentrations of PAMAM-GA conjugate for 12 h and subsequently, harvested and subjected to immunoprecipitation using an anti-Apaf-1 antibody. The immunoprecipitated complexes were subjected to western blotting for cytochrome c and Procaspase-9 to monitor the formation of the apoptosome complex. (D) After treating HCT 116 cells with mentioned concentrations of PAMAM-GA conjugate for 6 h, 12 h, and 24 h, the cells were harvested and the cell lysate was allowed to react with Z-DEVD-R110 substrate, followed by reading the fluorescence at an excitation and emission wavelength of 496 nm and 520 nm, respectively. The plot represents a fold increase in the caspase-3 activity compared to untreated control of the respective time points. Error bars represent mean \pm SEM from three independent experiments. * $p \leq 0.05$, ** $p \leq 0.01$ and *** $p \leq 0.001$ compared to untreated control cells.

mechanism of cell death. First, we examined the apoptotic cell death by Annexin V/Propidium Iodide staining. We noticed that HCT 116 cells treated with different concentrations of PAMAM-GA conjugate showed Annexin V and PI positive cells at 6, 12 and 24 h. The higher number of Annexin V and PI positive stained cells were found at 12 h. Further, we examined the expression of cell death regulatory proteins i.e. Bcl-2, cytochrome c, procaspase-3 and PARP in HCT 116 cells by western blotting. We observed that PAMAM-GA conjugate alleviates the expression of the anti-apoptotic protein, Bcl-2 as compared to the control and reduces levels of mitochondrial cytochrome c with a concomitant increase of the cytosolic cytochrome c, downregulation of pro-caspase3 and cleavage of PARP was found on shown time points (Figure 10(B)). The formation of the apoptosome complex was confirmed by co-immunoprecipitation (co-IP) assay. PAMAM-GA conjugate augments the interaction of pro-caspase-9, cytochrome c, and Apaf-1 in a dose-dependent manner, which indicating apoptosome mediated activation of caspase-9 and caspase-3. In consistent, we

found an increased activity of caspase-3 on PAMAM-GA conjugate treated HCT116 cells as compared to the control (Figure 10(D)).

PAMAM-GA conjugate losses of mitochondrial membrane potential (MMP)

Loss of mitochondrial membrane potential (MMP) is another indication of apoptosis. Here, we examined the loss of MMP using a mitochondria specific lipophilic fluorescent probe JC-1. When cells losses the MMP during apoptosis dye retains in the cytoplasm and fluoresces green, while in healthy cells, dye aggregates in the mitochondria and show red fluorescence. The quantitative analysis show that PAMAM-GA conjugate treated HCT-116 cells decrease in the ratio of red/green fluorescence to the control (untreated cells), which indicates HCT-116 cells treated with PAMAM-GA conjugate loss mitochondrial membrane potential (Figure 11(A)). In addition, microscopic analysis of the cells stained with JC-1 dye

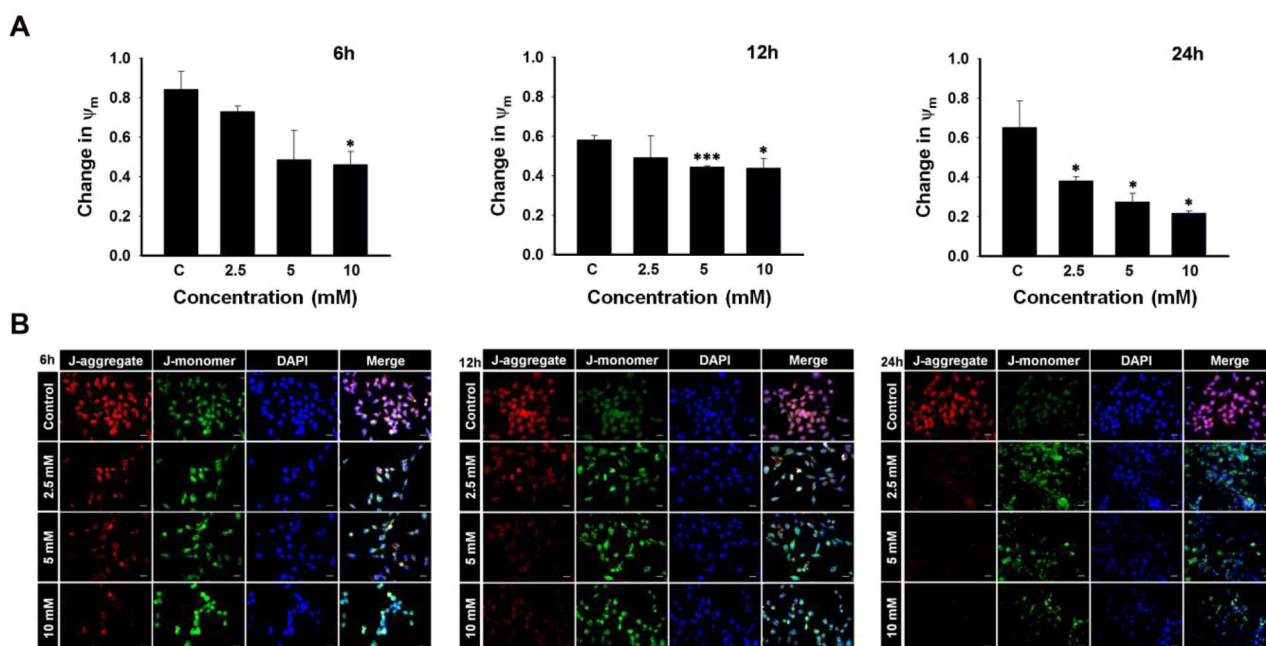


Figure 11. PAMAM-GA conjugate disrupts the mitochondrial membrane potential. HCT 116 cells were treated with 2.5 mM, 5 mM and 10 mM PAMAM-GA conjugate for indicated time and stained with JC-1 dye, followed by counterstaining with DAPI. The cells were analyzed under a fluorescence microscope. (A) Representative images of cells (B) The plots represent a quantitative change in the Mitochondrial Membrane Potential ($\Delta\Psi_m$). Scale bar: 20 μm . Error bars represent mean \pm SEM from three independent experiments. * $p \leq 0.05$, ** $p \leq 0.01$ and *** $p \leq 0.001$ compared to untreated control cells.

showed similar results (Figure 11(B)). These results suggest that GA conjugated with PAMAM dendrimer causes changes in mitochondrial membrane potential and executes mitochondrial-dependent apoptosis in HCT-116 cells.

Conjugation of GA with PAMAM dendrimer restricts necrotic cell death

First, we examined the toxic response from necrotic cell death of PAMAM-GA conjugate in HCT116 and NIH3T3 cells. We found negligible cytotoxicity (release of LDH) on PAMAM-GA conjugate treated HCT116 and NIH3T3 cells as compared to the free GA (Figure 12(A,B)). Next, we confirmed from qualitative analysis using Hoechst and PI staining. Results show that HCT 116 cells treated with GA for 6 h and 12 h showed intensified stained nuclei with both Hoechst and PI, which indicate necrotic cell death. However, HCT-116 cells treated with PAMAM-GA conjugate showed Hoechst-stained condensed nuclei with inadequate PI positive stained cells (Figure 12(D)). Lysosomal rupture is another indicative feature of necrotic cell death (Artal-Sanz et al., 2006). We monitored the lysosomal membrane integrity using LysoTracker red DND-99 dye counter stained with DAPI stain. We observed a progressive decrease in the intensity of red fluorescence of the dye in HCT 116 cells treated with free GA for 6 h and 12 h as compared to the control (untreated cells). Whereas, the cells treated with PAMAM-GA conjugate showed intense red fluorescence (Figure 12(C)). Collectively, these results suggest that at GA may induce cell death associated with necrosis whereas its conjugation with PAMAM dendrimer restricts cell death by necrosis and instigates apoptotic cell death in HCT 116 cells.

PAMAM-GA conjugate inhibits the activity of NF- κ B (p65) and release of pro-inflammatory cytokines IL-1 β and IL-6

Nuclear factor kappa B (NF- κ B) is a transcription factor that regulates expression of different sets of genes including proliferation, anti-apoptotic, inflammatory response for cell survival (Hayden & Ghosh, 2004) We examined the NF- κ B activation through cytosol to nuclear translocation of GFP tagged p65. The results show that PAMAM-GA conjugate inhibits the nuclear translocation of GFP tagged p65 (Figure 13(A)). This was further confirmed by western blotting analysis of p65 subunit. We observed a prominent cytosolic retention of p65 after treatment of PAMAM-GA conjugate for 6 h (Figure 13(B)). Thus, PAMAM-GA conjugate efficiently inhibits NF- κ B activity by restricting the cytosolic to nuclear translocation of p65 in HCT 116 cells. An elevated level of inflammatory cytokines is associated with the progression of malignancy (Landskron et al., 2014). PAMAM-GA treated HCT116 cells were tested for affect TNF- α induced secretion of the pro-inflammatory cytokines. The level of cytokines examined by ELISA indicates that PAMAM-GA conjugate efficiently reduces the secretion of IL-1 β and IL-6 (Figure 13(C, D)). In addition, expression of pro-inflammatory cytokines at transcriptional level was examined by real time PCR. The results show that PAMAM-GA conjugate treated cells downregulates the gene expression of IL-1 β and IL-6 mRNA in a dose-dependent manner as compared the control (Figure 13(E, F)).

Discussion

Polymer-drug conjugate is an emerging interest for drug delivery and manifests the efficacy of the drug with various advantages including improving the aqueous solubility,

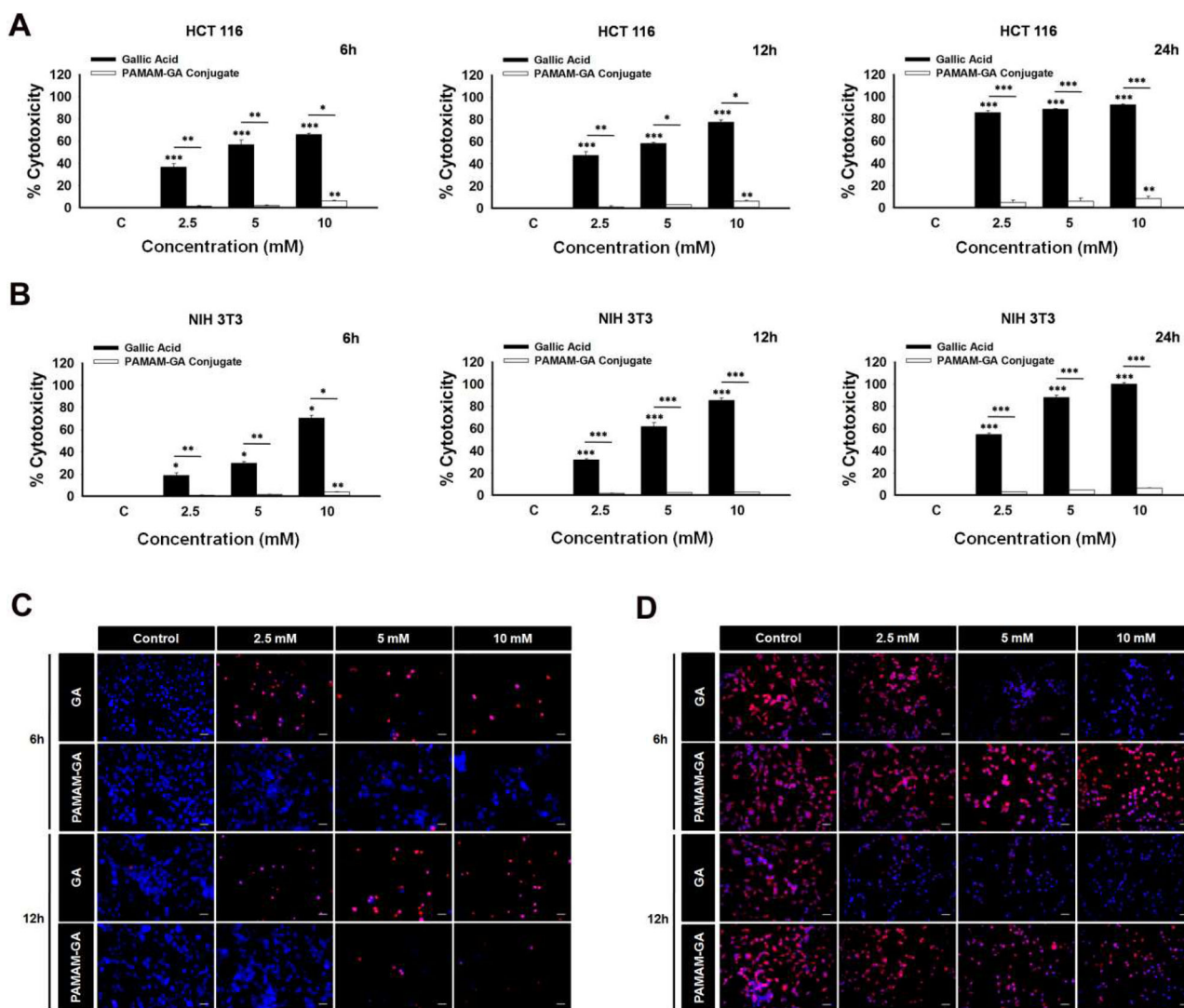


Figure 12. Effect of conjugation with PAMAM dendrimer on the cytotoxicity of GA. The percent of cytotoxicity was determined by measuring the intracellular LDH left after treatment of (A) HCT 116 and (B) NIH 3T3 cells with different concentrations of GA or PAMAM-GA conjugate for mentioned time points. (C) The lysosomal integrity was monitored in HCT 116 cells by staining the cells with LysoTracker Red DND-99 dye after treatment with indicated concentrations of GA and PAMAM-GA conjugate for 6 h and 12 h. The cells were counterstained with DAPI and analyzed under a fluorescence microscope. (D) Qualitative analysis of cytotoxicity was carried out in HCT 116 cells. The cells were treated with indicated concentrations of GA and PAMAM-GA conjugate for mentioned time points and subsequently stained with Hoechst 33342 dye and propidium iodide, followed by analysis under a fluorescence microscope. Scale bar: 20 μm . Error bars represent mean \pm SEM from three independent experiments. The difference is significant between GA and PAMAM-GA treatment groups at * $p \leq 0.05$, ** $p \leq 0.01$ and *** $p \leq 0.001$.

tissue distribution, sustained release and safety with reduced toxicity. Dendrimers are one of the unique, versatile and synthetic nanocarriers, which have an emerging interest in drug delivery due to flexible structural and functional properties (Akbarzadeh et al., 2018). The cellular uptake of dendrimers and dendrimer-based drug delivery systems is significantly greater than the linear polymeric carriers like polyethylene glycol (PEG), making them superior drug carriers (Khandare et al., 2006). It has been shown that dendrimers have a hydrophobic interior and hydrophilic chain, which allows solubilizing the hydrophobic drugs in the aqueous medium (Twyman et al., 1999). PAMAM dendrimers have emerged as excellent drug carriers because of large number of cationic groups on their surface provide multiple attachment sites and facilitate their uptake into the cells via 'proton sponge' mechanism (Sonawane et al., 2003). Moreover, they show great potential for *in vivo* targeting of tumors for therapeutic and diagnostic applications, as they exhibit enhanced

permeability and retention (EPR) effect. In this study, Gallic acid (GA) was conjugated with 4.0 GPAMAM dendrimers by the surface modification by taking into consideration that the conjugation of GA with the free amine groups of PAMAM dendrimer may reduce the cytotoxicity of dendrimer as well as enhance the bioavailability of GA.

The mechanistic conjugation of desired molecules or drugs with nanocarrier provides sustained release of the drug in a spatiotemporal manner to reduce its cytotoxicity and can improve the efficacy of drug (Lee & Yeo, 2015). Here, we examined the sustained release of GA from PAMAM-GA conjugate at physiological pH. We noticed that the slow release of GA from PAMAM-GA conjugate was found for an extended time as compared to the free GA. In addition, we examined the uptake of PAMAM-GA conjugate to monitor the intracellular accumulation of GA. We observed an increase concentration of GA in the cell lysates in a dose-dependent manner. Thus, this result suggests that

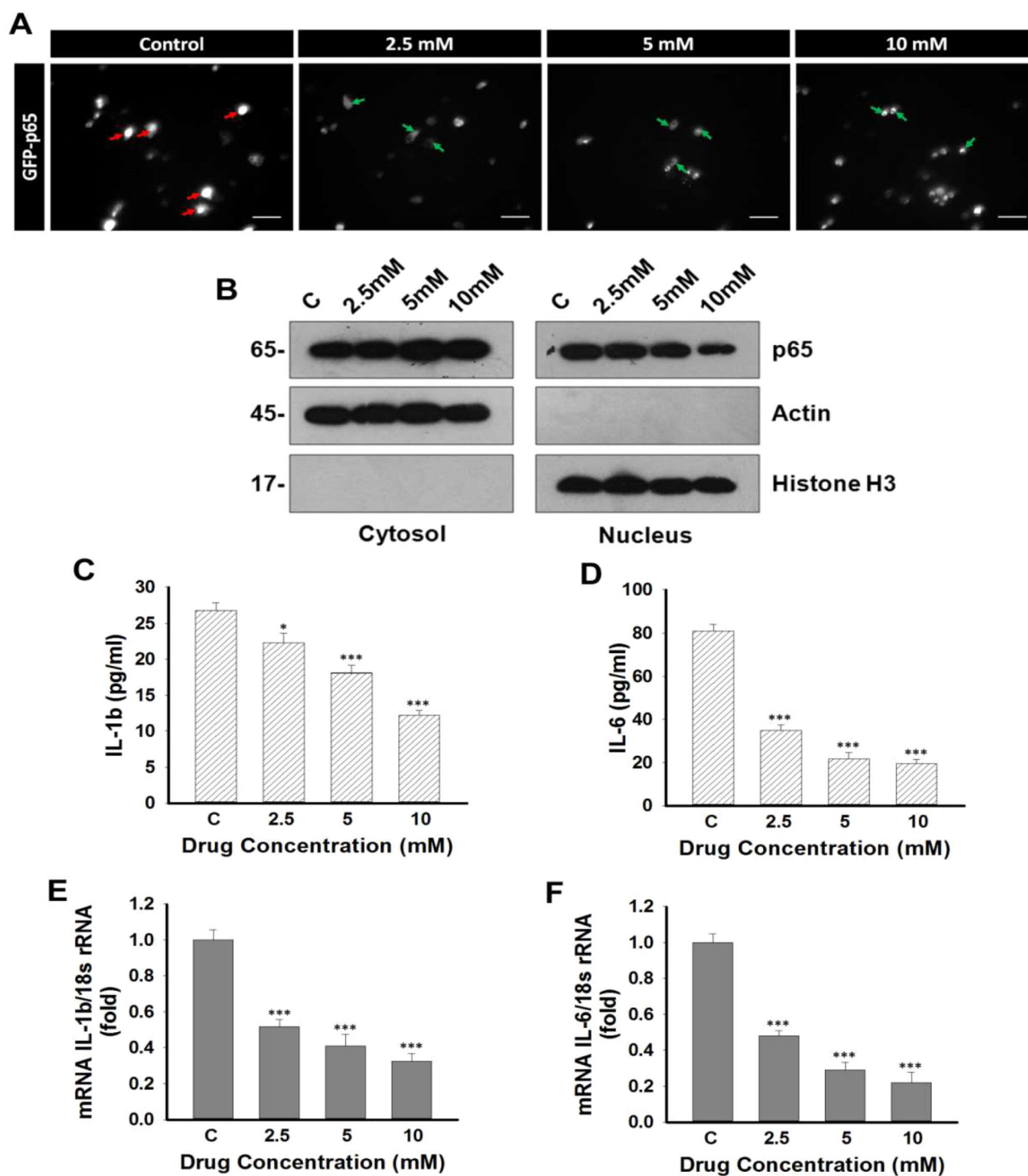


Figure 13. PAMAM-GA conjugate inhibits the NF- κ B (p65) activation and subsequent release of Pro-inflammatory cytokines. HCT 116 cells were treated with 2.5 mM, 5 mM and 10 mM PAMAM-GA conjugate for 6 h followed by TNF- α treatment for 1 h and analyzed for p65 translocation. (A) Microscopic analysis of GFP-p65 translocation under a fluorescence microscope. Scale bar: 20 μ m. (B) The western blots represent p65 expression in cytosol and nucleus. Actin and Histone H3 represent loading control. ELISA of released inflammatory cytokines (C) IL-1 β and (D) IL-6. RT-qPCR of inflammatory cytokines (E) IL-1 β and (F) IL-6. Error bars represent mean \pm SEM from three independent experiments. * $p \leq 0.05$ and *** $p \leq 0.001$ compared to untreated control cells.

PAMAM dendrimers may act as a carrier for the delivery of GA and intracellular internalization in HCT116 cells. First, we examined the IC_{50} value of GA and PAMAM-GA conjugate in cancer and normal cells using HCT 116 and NIH 3T3 cell lines. We found higher toxicity of free GA to HCT116 and NIH3T3 cells as compared to PAMAM-GA conjugate. Next, we observed the inhibition of cell proliferation on different origin of cancer cells. We found that PAMAM-GA conjugate

inhibits cell proliferation of different origin of cancer cells (HCT 116, HT-29, MCF-7). Interestingly, the inhibition of cell proliferation was negligible to the normal NIH3T3 cells, which indicates that conjugation of GA with PAMAM dendrimers manifest specificity towards cancer cells. Further, we confirmed the inhibition of cell survival by inhibiting the colony formation ability of HCT 116 cells. We observed that PAMAM-GA conjugate restricts colony formation ability of

HCT116 cells in a dose-dependent manner. Thus, the results indicate that the biological activity of GA and efficacy were improved and PAMAM-GA conjugate inhibits the proliferation of cancer cells. It is known that cancer cells have invasiveness and migration properties to spread the tumor. Here, we tested the migration ability of HCT-116 cells by wound healing scratch assay. We noticed that PAMAM-GA conjugate inhibits migration of HCT116 cells. Previous report suggests that secretion of MMP-9 enhances cell migration and angiogenesis (Mira et al., 2004). We noticed that treatment of PAMAM-GA conjugate diminished the expression of Pro-MMP-9.

PAMAM-GA conjugate significantly induces cell death, inhibits cell proliferation and migration of cancer cell. It was important to confirm molecular mechanism of cell death induced by PAMAM-GA conjugate. The results show that HCT 116 cells treated with PAMAM-GA conjugate showing Annexin V-FITC and PI positivity stained cells at lower concentrations at the earlier time points at 6–12 h. At 24 h, massive cell death was found. In continuation, we examined the expression of apoptosis regulatory proteins and found that decreased expression of anti-apoptotic protein Bcl-2 with subsequent activation of executioner caspase-3 and cleavage of PARP in PAMAM-GA conjugate treated HCT 116 cells. In addition expression of cytochrome-c was found to be down-regulated on mitochondrial fraction and upregulated in cytosolic fractions. Upon release, cytochrome c from mitochondria interacts with Apaf-1 and activates intrinsic signaling of apoptosis via the formation of apoptosome complex (Bratton & Salvesen, 2010). Immuno-precipitation and changes in mitochondrial membrane potential assays revealed that PAMAM-GA conjugate instigates apoptosome formation after the release of cytochrome-c from the mitochondria and activates executioner caspases for initiation of apoptotic cell death. Further, it was important to validate necrotic cell death. Cell death as a result of necrosis and developing resistance against apoptosis contributes to a major obstacle in cancer therapy (Krysko et al., 2017). Necrotic cell death is accompanied by the loss of plasma membrane integrity resulting in the leakage of intracellular milieu to the external environment and promotes metastasis in cancer (Lee et al., 2018). The previous report suggests that GA can induce calpain dependent necrotic cell death in hepatic stellate cells (Hsieh et al., 2014). Therefore, it was important to examine the effect of PAMAM-GA conjugate on necrotic cell death. The release of LDH is one of the considerable markers of necrotic cell death (Vaidya et al., 2019). We observed an elevated level of LDH after the treatment of GA to HCT 116 cells, but it was negligible after the treatment of the PAMAM-GA conjugate. In addition, we examined the effect on normal mouse fibroblast NIH 3T3 cells, which showed that the cytotoxicity of GA to the normal cells, but PAMAM-GA conjugate was showing negligible effect. Considering the pivotal role of necrosis as a “calpain-cathepsin hypothesis”, which postulates that the activation of calpain I instigates lysosomal rupture, which is the key step of rapid cell necrosis (Yamashima & Oikawa, 2009). Hence, we also examined the effect of GA and PAMAM-GA conjugate on the lysosomal

integrity in HCT 116 cells. We found that the cells treated with GA showed a prominent loss of lysosomal membrane integrity, but PAMAM-GA conjugate protect the lysosomal integrity. In concordance, the morphological assessment of the nucleus revealed that the cells treated with GA exhibit necrotic cell death. Whereas PAMAM-GA conjugate confers cell death via the mode of apoptosis. Thus, these results collectively indicate that the conjugation of GA with PAMAM dendrimer surmounts its apoptotic effects. Importantly, activation of NF- κ B and release of pro-inflammatory cytokines are prominent characteristics of the cancer cells (Xia et al., 2014). Here, we examined TNF- α primed activation NF- κ B and expression of pro-inflammatory cytokines IL-1 β and IL-6. Our results show that PAMAM-GA conjugate restricts cytoplasmic to nuclear translocation and expression of p65. Moreover, PAMAM-GA conjugate downregulated the expression of pro-inflammatory cytokines IL-1 β and IL-6 at protein and mRNA level.

Conclusion

Taken together, this study demonstrates that conjugation of GA with PAMAM dendrimers show sustained release of GA, which might facilitate to attain a steady-state therapeutic concentration of GA for an extended time. PAMAM-GA conjugate inhibits cell proliferation, improves cellular uptake of GA, inhibits colonogenic ability for cell survival, restricts cancer cell migration by down regulating the expression of MMP-9, inhibits NF- κ B activation and release of pro-inflammatory cytokines. PAMAM-GA conjugate augments mitochondria mediated apoptotic cell death in HCT 116 cells rather than necrotic cell death. On other hand PAMAM-GA conjugate showed negligible cytotoxic response as compared to the free Gallic acid to the normal cells. In conclusion, findings of this study revealed that PAMAM-GA conjugate improved the bioavailability of GA and directs the specificity toward cancer cells to manifest apoptotic cell death. This indispensable approach may be helpful for intervention of cancer therapy.

Acknowledgements

FT-IR and NMR analysis were carried out at CSMCRI, Bhavanagar, Gujarat, India. Authors acknowledge IAR, Puri Foundation for Education in India for providing junior Research Fellowship to KP, infrastructure facility and support. Department of Biotechnology, Gov of India is gratefully acknowledged for providing research grant to CP.

Authors contribution

Chandramani Pathak (CP): Conceptualization; Kavita Shirsath (KS), Khushbu Priyadarshi (KP), Bhargav Waghela (BW), Anupama Sharma (AS), Ajay Kumar (AK), Chandramani Pathak (CP): Methodology & Experimentation; CP, KS, KP, BW, AS: Data curation Software; KS, KP & CP: Writing and original draft preparation; KS, KP, BW & CP: Software and data validation; CP: Visualization, Investigation Supervision; CP: Writing- Reviewing and Editing.

Disclosure statement

The authors declare no conflict of interest.

Funding

This work was financially supported by the Department of Biotechnology, Ministry of Science & Technology, Government of India under Nano Science & Nanotechnology scheme (BT/PR14259/NNT/28/485/2010) to CP.

ORCID

Chandramani Pathak  <http://orcid.org/0000-0002-9389-8096>

References

- Akbarzadeh, A., Khalilov, R., Mostafavi, E., Annabi, N., Abasi, E., Kafshdooz, T., Herizchi, R., Kavetsky, T., Saghfi, S., Nasibova, A., & Davaran, S. (2018). Role of dendrimers in advanced drug delivery and biomedical applications: A review. *Experimental Oncology*, 40(3), 178–183. [https://doi.org/10.31768/2312-8852.2018.40\(3\):178-183](https://doi.org/10.31768/2312-8852.2018.40(3):178-183)
- Artal-Sanz, M., Samara, C., Syntichaki, P., & Tavernarakis, N. (2006). Lysosomal biogenesis and function is critical for necrotic cell death in *Caenorhabditis elegans*. *The Journal of Cell Biology*, 173(2), 231–239. <https://doi.org/10.1083/jcb.200511103>
- Badhani, B., Sharma, N., & Kakkar, R. (2015). Gallic acid: A versatile antioxidant with promising therapeutic and industrial applications. *RSC Advances*, 5(35), 27540–27557. <https://doi.org/10.1039/C5RA01911G>
- Bratton, S. B., & Salvesen, G. S. (2010). Regulation of the Apaf-1-caspase-9 apoptosome. *Journal of Cell Science*, 123(Pt 19), 3209–3214. <https://doi.org/10.1242/jcs.073643>
- Brglez Mojzer, E., Knez Hrnčić, M., Skerget, M., Knez, Z., & Bren, U. (2016). Polyphenols: Extraction methods, antioxidative action, bioavailability and anticarcinogenic effects. *Molecules*, 21(7), 901. <https://doi.org/10.3390/molecules21070901>
- Esfand, R., & Tomalia, D. A. (2001). Poly(amidoamine) (PAMAM) dendrimers: From biomimicry to drug delivery and biomedical applications. *Drug Discovery Today*, 6(8), 427–436. [https://doi.org/10.1016/S1359-6446\(01\)01757-3](https://doi.org/10.1016/S1359-6446(01)01757-3)
- Hayden, M. S., & Ghosh, S. (2004). Signaling to NF- κ B. *Genes & Development*, 18(18), 2195–2224. <https://doi.org/10.1101/gad.1228704>
- Hsieh, S.-C., Wu, C.-H., Wu, C.-C., Yen, J.-H., Liu, M.-C., Hsueh, C.-M., & Hsu, S.-L. (2014). Gallic acid selectively induces the necrosis of activated hepatic stellate cells via a calcium-dependent calpain I activation pathway. *Life Sciences*, 102(1), 55–64. <https://doi.org/10.1016/j.lfs.2014.02.041>
- Kahkeshani, N., Farzaei, F., Fotouhi, M., Alavi, S. S., Bahramsoltani, R., Naseri, R., Momtaz, S., Abbasabadi, Z., Rahimi, R., Farzaei, M. H., & Bishayee, A. (2019). Pharmacological effects of gallic acid in health and diseases: A mechanistic review. *Iranian Journal of Basic Medical Sciences*, 22(3), 225–237. <https://doi.org/10.22038/ijbms.2019.32806.7897>
- Kesharwani, P., Jain, K., & Jain, N. K. (2014). Dendrimer as nanocarrier for drug delivery. *Progress in Polymer Science*, 39(2), 268–307. <https://doi.org/10.1016/j.progpolymsci.2013.07.005>
- Khandare, J. J., Jayant, S., Singh, A., Chandna, P., Wang, Y., Vorsa, N., & Minko, T. (2006). Dendrimer versus linear conjugate: Influence of polymeric architecture on the delivery and anticancer effect of paclitaxel. *Bioconjugate Chemistry*, 17(6), 1464–1472. <https://doi.org/10.1021/bc060240p>
- Krysko, O., Aaes, T. L., Kagan, V. E., D'Herde, K., Bachert, C., Leybaert, L., Vandenebeele, P., & Krysko, D. V. (2017). Necroptotic cell death in anti-cancer therapy. *Immunological Reviews*, 280(1), 207–219. <https://doi.org/10.1111/imr.12583>
- Landskron, G., De la Fuente, M., Thuwajit, P., Thuwajit, C., & Hermoso, M. A. (2014). Chronic inflammation and cytokines in the tumor micro-environment. *Journal of Immunology Research*, 2014, 149185.
- Lee, J. H., & Yeo, Y. (2015). Controlled drug release from pharmaceutical nanocarriers. *Chemical Engineering Science*, 125, 75–84. <https://doi.org/10.1016/j.ces.2014.08.046>
- Lee, S. Y., Ju, M. K., Jeon, H. M., Jeong, E. K., Lee, Y. J., Kim, C. H., Park, H. G., Han, S. I., & Kang, H. S. (2018). Regulation of tumor progression by programmed necrosis. *Oxidative Medicine and Cellular Longevity*, 2018, 3537471. <https://doi.org/10.1155/2018/3537471>
- Manach, C., Williamson, G., Morand, C., Scalbert, A., & Remesy, C. (2005). Bioavailability and bioefficacy of polyphenols in humans. I. Review of 97 bioavailability studies. *The American Journal of Clinical Nutrition*, 81(1 Suppl), 230S–242S. <https://doi.org/10.1093/ajcn/81.1.230S>
- Medina, S. H., & El-Sayed, M. E. (2009). Dendrimers as carriers for delivery of chemotherapeutic agents. *Chemical Reviews*, 109(7), 3141–3157. <https://doi.org/10.1021/cr900174j>
- Mira, E., Lacalle, R. A., Buesa, J. M., de Buitrago, G. G., Jiménez-Baranda, S., Gómez-Moutón, C., Martínez-A, C., & Mañes, S. (2004). Secreted MMP9 promotes angiogenesis more efficiently than constitutive active MMP9 bound to the tumor cell surface. *Journal of Cell Science*, 117(Pt 9), 1847–1857. <https://doi.org/10.1242/jcs.01035>
- Ranjan, K., & Pathak, C. (2016). FADD regulates NF- κ B activation and promotes ubiquitination of cFLIP L to induce apoptosis. *Scientific Reports*, 6(1), 1–16. <https://doi.org/10.1038/srep22787>
- Sharma, A., Gautam, S. P., & Gupta, A. K. (2011). Surface modified dendrimers: Synthesis and characterization for cancer targeted drug delivery. *Bioorganic & Medicinal Chemistry*, 19(11), 3341–3346. <https://doi.org/10.1016/j.bmc.2011.04.046>
- Sherje, A. P., Jadhav, M., Dravyakar, B. R., & Kadam, D. (2018). Dendrimers: A versatile nanocarrier for drug delivery and targeting. *International Journal of Pharmaceutics*, 548(1), 707–720. <https://doi.org/10.1016/j.ijpharm.2018.07.030>
- Sinek, J., Frieboes, H., Zheng, X., & Cristini, V. (2004). Two-dimensional chemotherapy simulations demonstrate fundamental transport and tumor response limitations involving nanoparticles. *Biomedical Microdevices*, 6(4), 297–309. <https://doi.org/10.1023/B:BMMD.0000048562.29657.64>
- Sonawane, N. D., Szoka, F. C., & Verkman, A. (2003). Chloride accumulation and swelling in endosomes enhances DNA transfer by polyamine-DNA polyplexes. *The Journal of Biological Chemistry*, 278(45), 44826–44831. <https://doi.org/10.1074/jbc.M308643200>
- Svenson, S., & Tomalia, D. A. (2012). Dendrimers in biomedical applications—reflections on the field. *Advanced Drug Delivery Reviews*, 64, 102–115. <https://doi.org/10.1016/j.addr.2012.09.030>
- Tomalia, D. A., Baker, H., Dewald, J., Hall, M., Kallos, G., Martin, S., Roeck, J., Ryder, J., & Smith, P. (1986). Dendritic macromolecules: Synthesis of starburst dendrimers. *Macromolecules*, 19(9), 2466–2468. <https://doi.org/10.1021/ma00163a029>
- Twyman, L. J., Beezer, A. E., Esfand, R., Hardy, M. J., & Mitchell, J. C. (1999). The synthesis of water soluble dendrimers, and their application as possible drug delivery systems. *Tetrahedron Letters*, 40(9), 1743–1746. [https://doi.org/10.1016/S0040-4039\(98\)02680-X](https://doi.org/10.1016/S0040-4039(98)02680-X)
- Vaidya, F. U., Sharma, R., Shaikh, S., Ray, D., Aswal, V. K., & Pathak, C. (2019). Pluronic micelles encapsulated curcumin manifests apoptotic cell death and inhibits pro-inflammatory cytokines in human breast adenocarcinoma cells. *Cancer Reports*, 2(1), e1133. <https://doi.org/10.1002/cnr2.1133>
- Verma, S., Singh, A., & Mishra, A. (2013). Gallic acid: Molecular rival of cancer. *Environmental Toxicology and Pharmacology*, 35(3), 473–485. <https://doi.org/10.1016/j.etap.2013.02.011>
- Waghela, B. N., Sharma, A., Dhumale, S., Pandey, S. M., & Pathak, C. (2015). Curcumin conjugated with PLGA potentiates sustainability, anti-proliferative activity and apoptosis in human colon carcinoma cells. *PLoS One*, 10(2), e0117526. <https://doi.org/10.1371/journal.pone.0117526>
- Xia, Y., Shen, S., & Verma, I. M. (2014). NF- κ B, an active player in human cancers. *Cancer Immunology Research*, 2(9), 823–830. <https://doi.org/10.1158/2326-6066.CIR-14-0112>
- Yamashima, T., & Oikawa, S. (2009). The role of lysosomal rupture in neuronal death. *Progress in Neurobiology*, 89(4), 343–358. <https://doi.org/10.1016/j.pneurobio.2009.09.003>